Measuring Agglomerate Size Distribution and Dependence of Localized Surface Plasmon Resonance Absorbance on Gold Nanoparticle Agglomerate Size Using Analytical Ultracentrifugation

Justin M. Zook,[†,*] Vinayak Rastogi,[†] Robert I. MacCuspie,[†] Athena M. Keene,[‡] and Jeffrey Fagan[†]

[†]Material Measurement Laboratory, National Institute of Standards and Technology, Gaithersburg, Maryland 20899, United States, and [‡]Food and Drug Administration, Silver Spring, Maryland, United States

Agglomeration of nanoparticles (NPs) is frequently encountered when performing experiments with NPs in high ionic strength biological and environmental media. Sometimes agglomeration is driven intentionally, *e.g.*, for localized surface plasmon resonance (LSPR)-based[1−3] and surface-enhanced Raman spectroscopy (SERS)-based[2,4,5] biosensors, but it is also frequently undesirable, *e.g.*, before or during a nanotoxicity experiment.[6−10] In either context, characterization of the agglomerate size distribution and the coupled dependence of LSPR absorbance on agglomerate size is very challenging with conventional size measurement techniques. A key difficulty for many of the frequently used techniques is that the entire distribution of particles within a sample is concurrently sampled, and thus any differences in properties within the particle distribution are convoluted into the reported values. In contrast, analytical ultracentrifugation (AUC) allows dynamic monitoring of particle motion during spatial differentiation of particles according to their sedimentation coefficient, which increases with a particle's density and size. Because of this additional resolving power, AUC is typically used to characterize proteins and protein complexes, resolving important parameters such as the amount of hydration, size and shape, and rates of complexation.[11,12] Recently, however, the increased interest in NPs has led to a resurgence in its use to characterize unagglomerated NPs and their coatings.[13−16] Herein, we further extend the use of AUC to measuring two properties of NP agglomerates *in situ* in biological media:

ABSTRACT Agglomeration of nanoparticles during measurements in relevant biological and environmental media is a frequent problem in nanomaterial property characterization. The primary problem is typically that any changes to the size distribution can dramatically affect the potential nanotoxicity or other size-determined properties, such as the absorbance signal in a biosensor measurement. Herein we demonstrate analytical ultracentrifugation (AUC) as a powerful method for measuring two critical characteristics of nanoparticle (NP) agglomerates *in situ* in biological media: the NP agglomerate size distribution, and the localized surface plasmon resonance (LSPR) absorbance spectrum of precise sizes of gold NP agglomerates. To characterize the size distribution, we present a theoretical framework for calculating the hydrodynamic diameter distribution of NP agglomerates from their sedimentation coefficient distribution. We measure sedimentation rates for monomers, dimers, and trimers, as well as for larger agglomerates with up to 600 NPs. The AUC size distributions were found generally to be broader than the size distributions estimated from dynamic light scattering and diffusion-limited colloidal aggregation theory, an alternative bulk measurement method that relies on several assumptions. In addition, the measured sedimentation coefficients can be used in nanotoxicity studies to predict how quickly the agglomerates sediment out of solution under normal gravitational forces, such as in the environment. We also calculate the absorbance spectra for monomer, dimer, trimer, and larger gold NP agglomerates up to 600 NPs, to enable a better understanding of LSPR biosensors. Finally, we validate a new method that uses these spectra to deconvolute the net absorbance spectrum of an unknown bulk sample and approximate the proportions of monomers, dimers, and trimers in a polydisperse sample of small agglomerates, so that every sample does not need to be measured by AUC. These results demonstrate the potential utility of AUC to characterize NP agglomeration and sedimentation for nanotoxicity and biosensor studies, as well as to characterize NP agglomerate size and absorbance to improve LSPR and surface-enhanced Raman spectroscopy based biosensors.

KEYWORDS: gold colloid · aggregate · analytical ultracentrifugation · nanoparticle toxicity · biosensors

(1) the agglomerate size distribution, and (2) the individual LSPR absorbance spectra of agglomerates. Both of these measurements improve understanding of nanotoxicity and LSPR-based colorimetric biosensors.

For NP agglomerates, conventional methods used to characterize the size distribution of unagglomerated NPs become more difficult. Conventional methods are subject to measurement artifacts (*e.g.*, microscopies), or
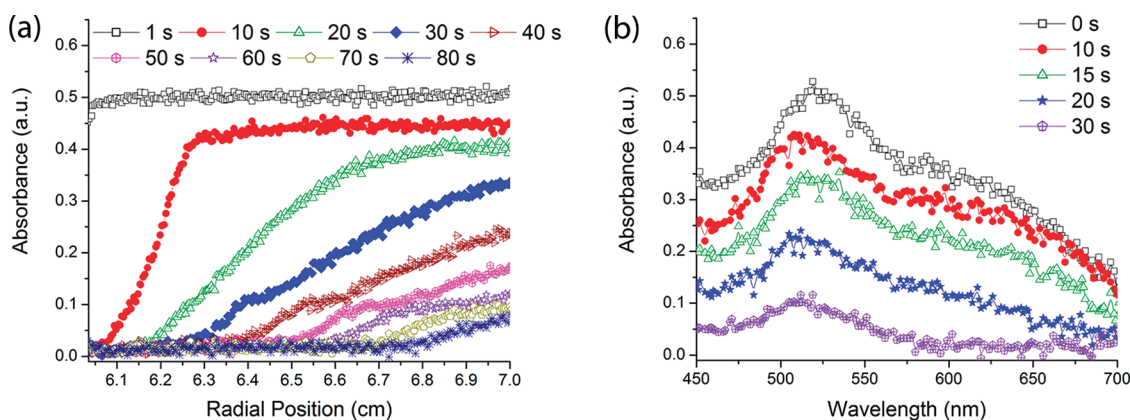
Figure 1. (a) Example of AUC radial scan measurements of a sample containing 30 nm AuNPs agglomerated for 2 s with absorbance measured at 526 nm. These measurements were used to calculate the size distribution of the agglomerates in the sample from the changes in position and shape of the sedimentation boundary over time. The NPs were sedimenting from left to right under a mean relative centrifugal force of 291g (2000 rpm). (b) Example of AUC wavelength scan measurements of a similar sample containing 30 nm AuNPs agglomerated for 2 s at the radius 6.8 cm. The time derivative at each wavelength was used to calculate how the absorbance spectrum depends on size. The NPs were sedimenting under a mean relative centrifugal force of 455g (2500 rpm).

they measure a mean size and assumptions must be made to estimate the size distribution (*e.g.*, dynamic light scattering (DLS)). Electron and probe microscopy techniques are frequently used to characterize unagglomerated NPs, but careful sample preparation procedures are required when measuring agglomerates because additional agglomeration, or agglomerate rupture, can occur during drying.[17−19] Microscopy techniques are thus rarely used to provide quantitative size distributions of agglomerates and, when used, must be rationalized due to a lack of knowledge of artifacts from the deposition process, flattening of the deposited agglomerate on the surface, and the time-intensive nature of particle-by-particle measurements. In our previous work, we used diffusion-limited colloidal aggregation (DLCA) theory in combination with the mean size measured by DLS to overcome limitations in estimating broad size distributions of agglomerates from DLS alone.[10] DLCA theory was shown previously to explain the increase in mean diameter during diffusion-limited aggregation,[20] but the size distribution has not been verified experimentally. Here, we compare the theoretical DLS−DLCA size distributions to the AUC experimental distributions in order to determine how accurately the much simpler DLS−DLCA method estimates the distribution. Other techniques such as field flow fractionation have also recently been used to separate small NP clusters in simple aqueous solutions,[21] but they have not been used for larger agglomerates and the quality of separations can be degraded by membrane−NP interactions in complex biological media. AUC is therefore advantageous in that it differentially sediments NP agglomerates by size in complex media without using a membrane, while simultaneously allowing measurement of the absorbance spectrum as a function of agglomerate size.

After measuring the size distribution of AuNP agglomerates using AUC, we then used AUC in wavelength

scan mode (effectively acting like a UV−visible spectrophotometer) to measure the LSPR absorbance spectra of individual agglomerate sizes. Since it was observed that agglomeration of gold and silver NPs causes a red-shifted peak to develop in the LSPR absorbance, colorimetric biosensors based on LSPR absorbance changes have been increasingly used to detect various analytes. Thus, understanding how the spectra depend on agglomerate size is a step toward improving LSPR-based biosensors. Such sensors work based on the fact that when ligands are attached to AuNPs and AgNPs, their agglomeration rate can be controlled by a specific analyte. To detect specific analytes, different ligands are attached, such that color changes can be induced by DNA−DNA, aptamer−protein, antibody−antigen, and lectin−carbohydrate binding.[1−3] Measuring the number of biosensing NPs bound into the agglomerates more precisely will improve the precision of the analyte detection. Various theories (*e.g.*, discrete dipole approximation, or DDA) have been developed to explain the changes in LSPR spectra during the agglomeration process, but they have been difficult to verify experimentally due to the bulk measurement of the net absorbance of broad size distributions of NP agglomerates.[22,23] A few single-particle techniques have been developed, but require measurement cluster-by-cluster.[24] Here, we continuously scan across the absorbance spectrum while the AuNP agglomerates are sedimenting and are thereby able to measure *in situ* in biological media the individual spectra of monomers, dimers, trimers, and larger agglomerates up to 600 NPs. Finally, the measured absorbance spectra of monomers, dimers, and trimers are used to calculate each of their concentrations simply from the bulk absorbance of a polydisperse sample of small agglomerates.
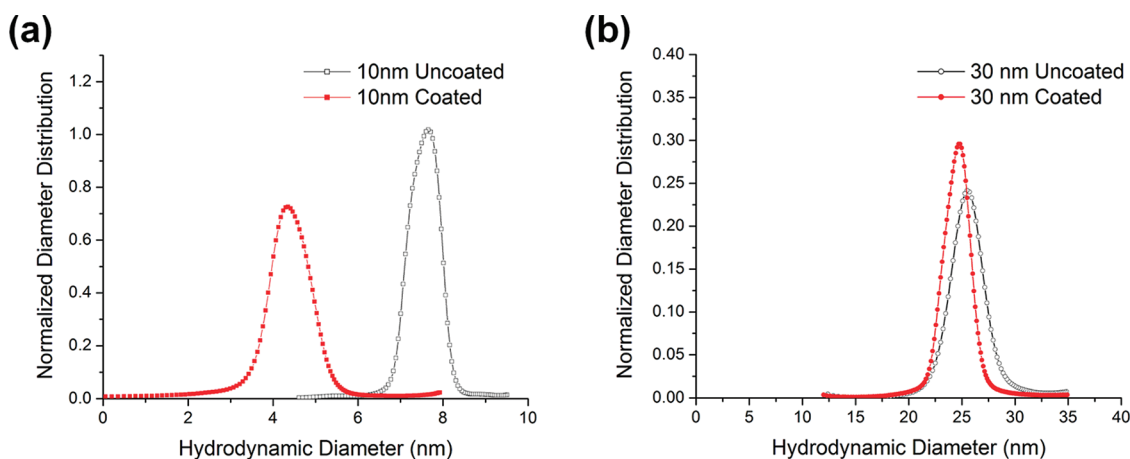
(a)

(b)

Figure 2. Size distributions calculated from AUC radial scan measurements for (a) nominally 10 nm AuNPs and (b) nominally 30 nm AuNPs dispersed in deionized water (gray) and in the cell culture media DMEM + 1% BSA (red). For NPs dispersed in BSA, the distributions are compensated for a monolayer BSA coating, and the monolayer BSA thickness is subtracted from the hydrodynamic diameter, so the reported diameters are for the naked AuNPs. Distributions are normalized so the area under the curve is 1.

RESULTS/DISCUSSION

We used AUC to measure properties of the sedimenting AuNP agglomerates in two modes: (1) To measure agglomerate size distributions, we used the more common radial scan mode. In this mode, the AUC repeatedly scans across all radial positions in the cell at a single wavelength during the sedimentation process, resulting in absorbance traces such as those in Figure 1a. The cell is initially uniformly filled with NP agglomerates; due to the applied centrifugation, the agglomerates sediment with time, with larger agglomerates sedimenting more quickly, leading to the movement and spreading of the boundary visible in the figure. The shape and time dependence of the boundary contains the information about the NP agglomerate size distribution. (2) To measure the LSPR absorbance of individual agglomerate sizes, we used the wavelength scan mode. In this mode, the AUC repeatedly scans across a spectrum of wavelengths at a single radius, resulting in time-dependent absorbance traces such as those in Figure 1b.

Agglomerate Size Distributions from AUC. We used the AUC in radial scan mode to demonstrate that we could measure the particle size distributions and agglomerate size distributions of nominally 10 and 30 nm AuNPs. We measured the size distributions of systems with increasing levels of complexity: (1) uncoated AuNPs in water, (2) bovine serum albumin (BSA)-coated singly dispersed AuNPs in cell culture media (DMEM), and (3) BSA-coated AuNP agglomerates with mean sizes ranging from well-dispersed AuNPs to a few hundred nanometers. The theories we developed to calculate the size distributions from the measured sedimentation coefficient distributions are described below in the Materials/Methods section and in the Supporting Information.

Initial measurements were used to establish the size distributions of unagglomerated nominally 10 and 30 nm AuNPs in water without a BSA coating and in cell culture media with a BSA coating. Figure 2 compares the AUC size distributions of the AuNPs in water to BSA-coated AuNPs in DMEM−BSA (calculated using the analysis software Sedfit,[12,25] after compensating for a BSA monolayer coating as described in the theory and Supporting Information). Both nominally 10 and 30 nm AuNPs had narrow size distributions around measured mean sizes of 7.6 and 25.6 nm, respectively. These values compare well with the independently determined values from atomic force microscopy (AFM) particle height measurements of 7.1 ± 2.7 and 28.0 ± 6.1 nm (mean ± standard deviation), respectively. For the AUC measurements, 80% of the NPs (based on absorbance) were within 0.8 nm of the mean size of the 10 nm AuNPs and within 4.0 nm of the mean size of the 30 nm AuNPs. AFM measurements of dried AuNPs indicated an increase in mean size of 1.4 nm for both sizes of AuNPs when coated with BSA, which is smaller than expected on the basis of the size of BSA. However, this difference is reasonable because the samples were dehydrated for AFM measurements (see Figure S6 in the Supporting Information for all AFM size distributions). The decrease in sedimentation coefficients after BSA coating shown in red in Figure 2 cannot be completely explained by a single monolayer of BSA for either 10 or 30 nm AuNPs. However, the difference in mean diameters between uncoated and BSA-coated NPs was only about 4% for 30 nm AuNPs. In addition, our assumption of a densely coated BSA monolayer is only an approximation, and small changes in the density or thickness can significantly affect the estimated size of the BSA-coated 10 nm AuNPs. Fortunately, this assumption has little effect on the size estimates of agglomerated NPs because the agglomerate sizes are much larger than the coating thickness.
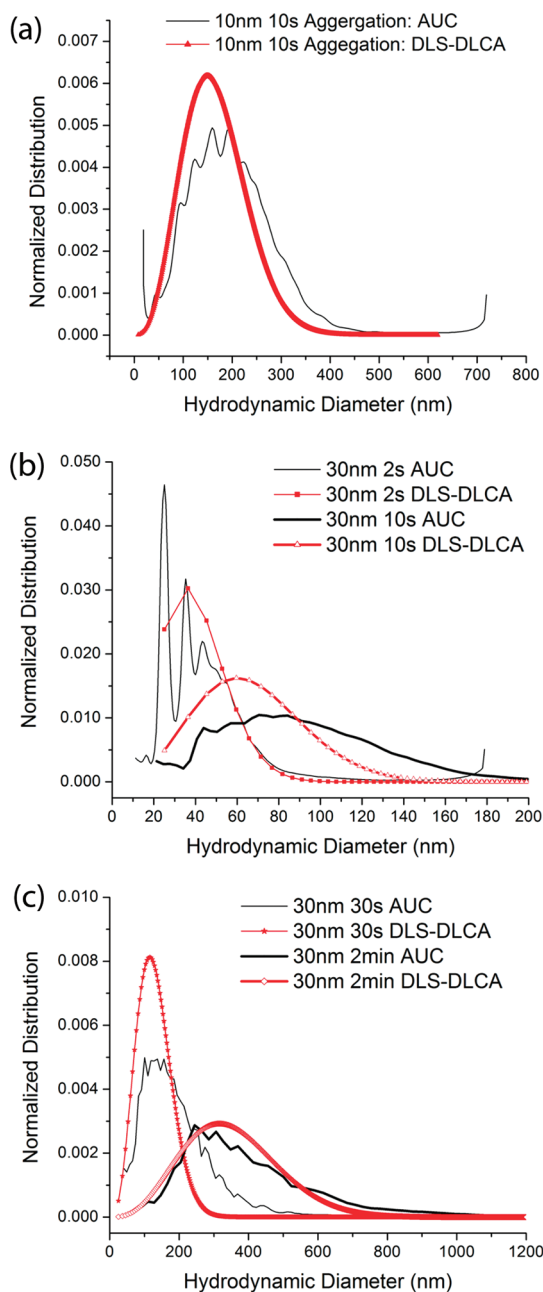
(a)

(b)

(c)

Figure 3. Comparison of the absorbance-weighted agglomerate size distributions measured by AUC (lines without data points) using $c(s)$ regularization to the mass-weighted size distributions calculated from the DLS mean diameter using DLCA theory (lines with data points). Each data point (triangle or circle) on the DLS−DLCA curves represents a single number of NPs/agglomerate (M), where the left-most point represents $M = 1$. (a) Distributions for 10 nm AuNPs agglomerated for 10 s. (b) Distributions for 30 nm AuNPs agglomerated for 2 s (thin lines) and 10 s (thick lines). (c) Distributions for 30 nm AuNPs agglomerated for 30 s (thin lines) and 2 min (thick lines). Distributions are normalized so the area under the curve is 1.

To test the effectiveness of AUC for the NP agglomerates, agglomerates of AuNPs with different mean sizes were produced by driving agglomeration of the primary NPs in DMEM for different periods of time prior to the addition of BSA using recently described
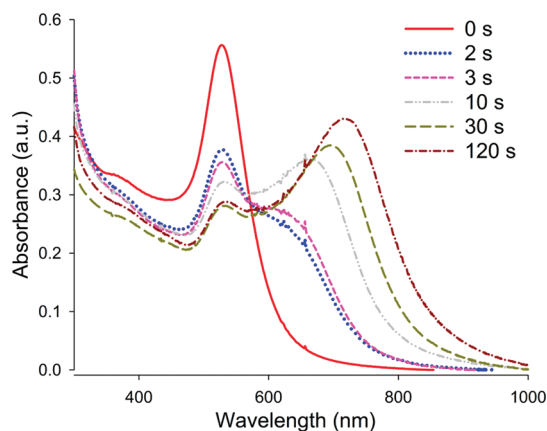

Figure 4. Example of how agglomeration changes the bulk absorbance spectra. Absorbance spectra of 30 nm AuNPs agglomerated for 0, 2, 10, 30, and 120 s before introduction of BSA. The measured resulting mean diameters, from AUC, are 25, 48, 98, 220, and 540 nm, respectively.

methods.[10] The addition of BSA terminates the agglomeration of the NPs and thus can be used to control the average final agglomerate size. The polydisperse agglomerates of the nominally 10 and 30 nm primary AuNPs were then measured in the AUC in radial scan mode to determine the size distribution of the agglomerates. Figure 3 compares the absorbance-weighted size distributions calculated from AUC (compensated for BSA coating) to the mass-weighted size distributions calculated from DLCA theory. The DLCA theory was used in conjunction with the mean diameter measured by DLS and compensated for vibration and rotation of the agglomerates, as described in the Theory section and in the Supporting Information. DLCA theory best matches the AUC size distributions for the largest 10 and 30 nm agglomerates. However, in general, the AUC size distribution was broader than the theoretically predicted distribution. A broader size distribution may be explained by the agglomeration process not being completely diffusion-limited, since the opposite extreme of reaction-limited agglomeration results in much broader size distributions. Previous work showed that in the presence of contamination the agglomeration rate was slower than predicted by diffusion-limited aggregation theory.[20] Therefore, it is not surprising that the complex composition of cell culture media could also slow agglomeration and result in broader size distributions than expected by DLCA. One caveat for the AUC measurements of the smallest agglomerate sizes is that the absorbance at 526 nm depends significantly on agglomerate size, decreasing as agglomeration increases, as shown in Figure 4. This dependence of absorbance on agglomeration causes the proportion of monomers to be overestimated, which is consistent with the AUC distributions when compared with the DLS−DLCA distributions marked by circles in Figure 3b. However, as we demonstrate in Figure 4 and in the next section, the
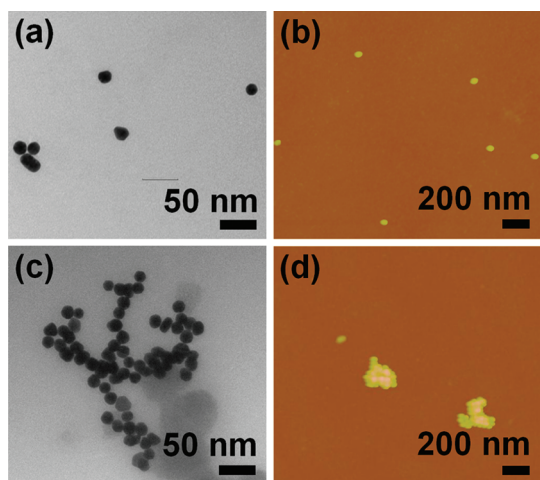
(a) 50 nm **(b)** 200 nm **(c)** 50 nm **(d)** 200 nm

Figure 5. Representative images of unagglomerated (0 s, a and b) and agglomerated (30 s, c and d) ~30 nm AuNPs measured by TEM (a and c) and AFM (b and d). The Z color scale in (b) and (d) is 0 to 75 nm.

absorbance at 526 nm has only a weak dependence on agglomerate size for larger agglomerates, so that the Mie effect apparently does not have a significant influence on the absorptivity of our large agglomerates. Even for small agglomerates, the absorbance depends much less on size than light scattering, which is used by many other size measurement methods. Therefore, AUC can still generally provide a more reliable size distribution than DLS-DLCA or other bulk measurement methods because agglomerates are differentially sedimented by size.

The sedimentation coefficient distributions measured by AUC (*e.g.*, Figures S2a and S3 in the Supporting Information) can also be used to predict sedimentation rates of different sizes of NP agglomerates in environmental and biological systems. These rates are especially relevant to studying nanotoxicity in environmental systems, in which larger NP agglomerates will settle more rapidly to the bottom. Sedimentation velocities can be calculated from sedimentation coefficients using the equation $s = u/a$, where s is the sedimentation coefficient, u is the sedimentation velocity, and a is the acceleration (usually 9.8 m/s^2 from gravity in environmental systems). For example, for 30 nm NPs agglomerated for 2 min, our measured sedimentation coefficients predict that the median agglomerate size (370 nm) will sediment in gravity at a rate of 0.70 cm/day, but 20% of the mass of the total agglomerates in the same sample will sediment more slowly than 0.35 cm/day or more quickly than 1.5 cm/day. These measured sedimentation coefficient distributions can help predict how quickly NP agglomerates will be deposited on the bottom of rivers or lakes, where they pose different nanotoxicity risks.

To verify the presence of agglomerates and gain information about their structures, transmission electron microscopy (TEM) and AFM images were taken of

the unagglomerated and 30 s agglomerated 30 nm AuNP samples. Figure 5a shows representative structures in the unagglomerated, 0 s, sample measured by TEM, with primarily single particles but a few small agglomerates (which may result from drying of the sample onto the substrate). This result is consistent with the monomodal distribution of BSA-coated AuNPs in Figure 2b. Figure 5c shows representative agglomerates in the 30 s sample measured by TEM, with mostly fractal-like structures but a few that are partially chain-like. To confirm that the agglomeration observed by TEM was not primarily due to drying of the sample onto the substrate, AFM images were taken of the NPs electrostatically attached to positively charged substrates so that additional agglomeration would not occur due to drying the sample on the substrate (see Materials/Methods). Figures 5b and d show representative structures observed by AFM for unagglomerated 0 s and agglomerated 30 s samples. The structural form of the agglomerates can affect sedimentation coefficients, and it has an even larger effect on estimates from methods based on light scattering such as DLS. Therefore, some of the difference between AUC and DLS/DLCA size distributions could result from inaccurate estimates of the fractal dimension. The agglomerate structure can also influence the absorbance spectrum, which we examine next with AUC.

Dependence of Absorbance Spectrum on Agglomerate Size. Since it is not possible to measure the absorbance spectra of individual monodisperse agglomerate sizes using bulk absorbance methods, we used AUC to scan wavelengths across the visible spectrum over time during the sedimentation process. In the absence of diffusion or other dispersion, each agglomerate size will form a sharp sedimentation boundary that moves from the inside of the centrifugal cell to the outside. When measuring the absorbance spectra at a single position, the contributions to the measured absorbance from each agglomerate size will cease as its sedimentation boundary crosses that position. Therefore, we can calculate the absorbance spectrum of various agglomerate sizes from the time derivative of the measured absorbance. The methods and theory are described in detail in the Theory section and in the Supporting Information.

To measure the spectra across a broad range of agglomerate sizes, we created nine samples with mean sizes ranging from single 30 nm AuNPs to an approximate mean agglomerate size of 370 nm (measured by DLS, compensated for vibration and rotation). We then took the average measured spectra of various distinct agglomerate sizes (clusters of $M = 1$, 2, 3, 4, 7, 10, *etc.*, 600 NPs) for the agglomerated samples that contained sufficient quantities of the specified size to get a good signal-to-noise ratio, which is shown in Figure 6a. The cluster sizes were estimated from the sedimentation coefficients as described in the
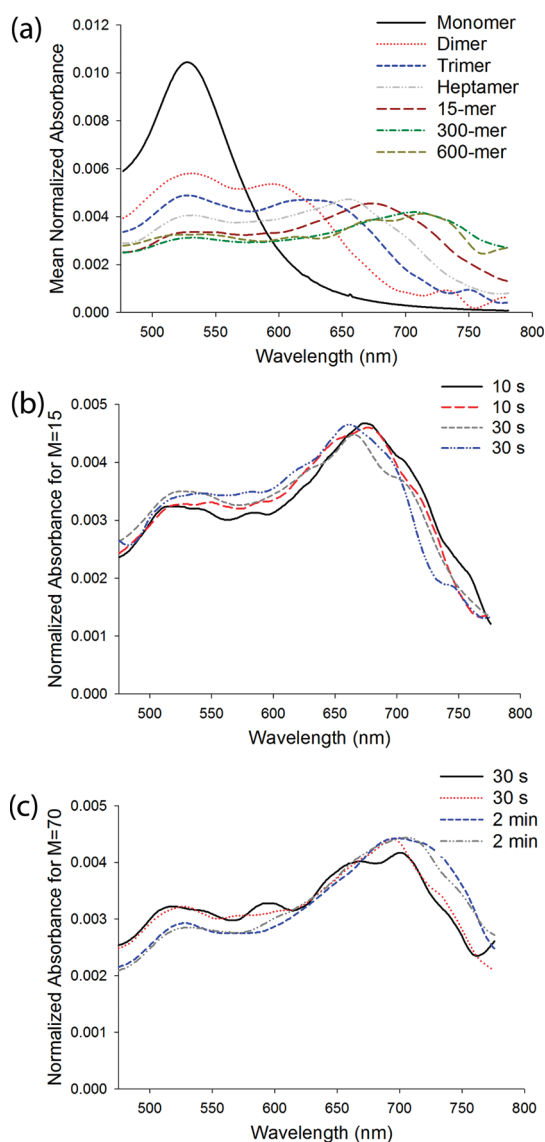
Figure 6. (a) Absorbance spectra of different sizes of monodisperse agglomerates containing different numbers of 30 nm AuNPs (1, 2, 3, 7, 15, 50, or 300 AuNPs), calculated from AUC measurements of polydisperse agglomerates. Spectra were calculated from solutions containing different mean sizes of agglomerates in DMEM + 1% BSA and were normalized to have an area under the curve equal to 1. (b) Normalized absorbance spectra for agglomerates containing 15 NPs from the 10 and 30 s agglomerated samples. (c) Normalized absorbance spectra for agglomerates containing 70 NPs from the 30 s and 2 min agglomerated samples.

Materials/Methods and in the Supporting Information. The absorbance peak at 526 nm decreased dramatically compared to monomers even for dimers ($M = 2$) due to coupling of LSPR between the NPs, and it continued to decrease until reaching a size of about $M = 15$. Agglomerates maintain a significant absorbance peak at 526 nm, possibly due to incomplete LSPR coupling between all NPs within the agglomerate. In contrast, the absorbance at 700 nm due to coupling between multiple NPs increases from near zero for unagglomerated NPs to near its maximum for $M \geq 15$. In addition,

the red-shifted peak shifted to increasingly longer wavelengths for increasing agglomerate sizes until reaching a maximum of ∼710 nm for agglomerates with $M \geq 30$. In summary, agglomerates maintain a significant absorbance peak around 526 nm (possibly due to incomplete lSPR coupling between all NPs within the agglomerate), although this peak decreases rapidly until it reaches about one-third of the monomer peak. Simultaneously, the agglomerates develop a second red-shifted peak that shifts to longer wavelengths with increasing agglomerate size.

Several small sources of uncertainty exist for these absorbance spectra. (1) The absorbance spectra were normalized so that the area under the curve is 1. (2) Due to diffusion and other dispersion, the absorbance spectrum may not correspond to a single monodisperse agglomerate size. However, for large agglomerates, the diffusion coefficient is extremely small, and the absorbance does not depend strongly on size. Even for small agglomerates, diffusion is small on the time scale of the experiment (see Supporting Information) and is therefore expected to add only a small uncertainty to the M values assigned to the spectra. (3) The protein coating causes a small shift in the primary peak of the LSPR spectrum, but the LSPR spectral changes observed in this work are primarily due to interactions between AuNPs within the agglomerate. (4) All agglomerates larger than monomers and dimers can have multiple structures, which can affect their absorbance spectra[26] as well as their sedimentation coefficients, so that some structural information should be known. In this study, to calculate M from the sedimentation coefficient, we assume that the fractal dimension of the agglomerates is 1.86, which was measured previously for DLCA.[20] Deviations from the fractal dimension would affect the values of M in Figure 6. However, AUC is not unique in this respect, as most measurements of agglomerates require assumptions about structure of the agglomerates. As long as these small sources of uncertainty are understood, AUC provides a valuable, unique method to measure the absorbance spectra of a wide range of agglomerate sizes.

To determine whether the structure of the AuNP agglomerates changes with increasing agglomeration times (i.e., increasing mean agglomerate size), we next measured if the absorbance spectra of the same agglomerate size depends on the mean agglomerate size of the sample. When comparing the absorbance spectra of single agglomerate sizes in samples with different mean agglomerate sizes, the spectra were generally similar for small agglomerates of a few NPs (see Figure 6b), but sometimes differed subtly for larger agglomerates (see Figure 6c). Specifically, agglomerates taken from samples with a larger mean size often had a larger red-shifted peak than the same size of agglomerates from a population with a smaller mean size. The reason for this difference is unclear, but we
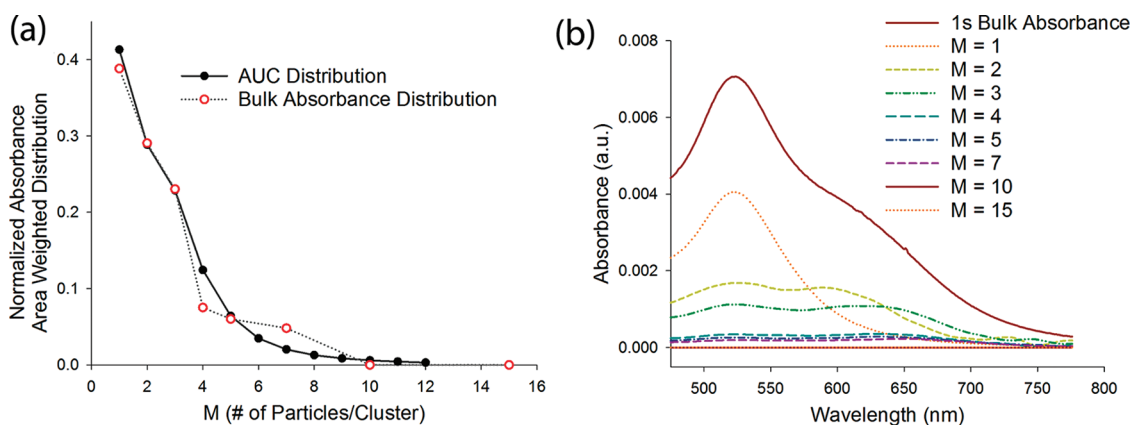
Figure 7. (a) Comparison of the agglomerate size distribution measured by AUC (black squares) to the distribution calculated simply from the bulk absorbance using a traditional UV—visible spectrophotometer and the data in Figure 6 (red circles). The 30 nm AuNPs were agglomerated for ~1 s in cell culture media before adding BSA. (b) Bulk absorbance spectrum and its component spectra from each agglomerate size for the same sample as in (a).

speculate that it could result from somewhat different agglomerate structures for the two populations. Therefore, although we are measuring the spectra of nearly monodisperse agglomerates in terms of having the same sedimentation coefficient, agglomerates with the same sedimentation coefficient (except for dimers) can have different structural arrangements of the NPs or even different numbers of NPs/agglomerate. However, again this limitation is not worse than for other techniques, as most measurement methods require assumptions about the structure of agglomerates, since structure affects light-scattering properties, and most microscopy techniques cannot measure the three-dimensional structures in a solution.

Calculating the Size Distribution of Small Agglomerates from the Bulk Absorbance. A useful application for knowledge of the size dependence of the absorbance spectrum from the AUC measurement is the potential for estimating the size distribution in samples not measured by AUC directly from deconvoluting their bulk absorbance spectrum. Advantages of using the bulk absorbance without separation techniques would be the much simpler methodology and higher time resolution of modern UV—visible spectrophotometers than DLS or AUC instruments, as well the much greater prevalence of UV—vis instruments than the other techniques. In addition, unlike DLS, deconvolution of the absorbance spectrum could provide proportions of each discrete size of agglomerate. Thus, calculations for the size distribution of populations of small agglomerates from their bulk absorbance spectrum were made for additional samples based on our measured spectra of each agglomerate size reported in Figure 6. Since the spectra change the most for the smallest agglomerates, we anticipate that this method for calculating the size distribution from the bulk absorbance spectrum will be most accurate in the limit of small amounts of agglomeration. We calculated the agglomerate size distribution by finding the optimal

combination of small agglomerates that sum to the bulk absorbance spectrum (see Figure 7b for an example and the Theory section below for detailed calculations). To test the accuracy of this method, we compared the size distribution estimated from the bulk absorbance spectrum to the size distribution measured by AUC (calculated from the area under the AUC absorbance curves to minimize biases resulting from the dependence of absorbance on agglomeration). Figure 7a shows that for very small agglomerates (agglomerated for 1 s), the bulk absorbance spectrum can be used to achieve a very good estimate of the actual size distribution, especially for monomers, dimers, and trimers, for which the differences were less than 6%. Figure 7b shows how the absorbance of each agglomerate size contributes to the bulk absorbance. However, for slightly larger agglomerates (agglomerated for 2 s), the size distribution calculated from the bulk absorbance spectrum tends to significantly overestimate the size of agglomerates (see Figure S5). This result is understandable because the absorbance is much less dependent on agglomerate size for large agglomerates, and thus it is more difficult to generate an accurate projection of the size distribution for samples containing large agglomerates. Structural differences within agglomerate sizes larger than dimers may also affect both the sedimentation coefficients and the absorbance spectra, so the resulting size distributions should be treated only as proportions of the representative structure of each agglomerate size. It should be noted that for validation purposes these agglomeration times were relatively short because they were in the high ionic strength DMEM without stabilizing agents. More useful applications of this method might be measuring the small amount of agglomeration observed when dispersing NPs at a high concentration in the presence of a stabilizer such as BSA[10] or monitoring changes in small NP agglomerates when they are not completely stabilized. Therefore, once AUC is used to measure the absorbance spectra of each

agglomerate size, the bulk absorbance appears to be a promising rapid method to estimate agglomerate size distribution as long as most of the agglomerates contain less than five to six NPs.

CONCLUSIONS

Analytical ultracentrifugation is an effective tool for measuring the size distribution of NP agglomerates, as well as for measuring the dependence of the absorbance spectrum on agglomerate size. We demonstrated that AUC has sufficient resolution that peaks for monomers, dimers, and trimers are separated for small agglomerates and that larger agglomerates can be measured up to a few hundred nanometers in size. Although sources of uncertainty exist in AUC measurements of agglomerates, including assumptions about BSA coating density, agglomerate structure, and uniform absorbance, most of these uncertainties can likely be minimized in most potential applications. Furthermore, these same sources of uncertainty, or other larger sources of uncertainty, also exist when measuring agglomeration with competing methods such as methods based on microscopy, light scattering, or other separation techniques such as field flow fractionation. For the first time, we validated a method to measure the absorbance spectra of a wide range of distinct sizes of agglomerates of AuNPs, which we also demonstrate to be useful for characterizing small agglomerates simply from the bulk absorbance.

While DLS and aggregation theory can be used to obtain a rough estimate of agglomerate size distribution,

AUC measurements also demonstrated that the size distributions of agglomerated NPs are generally broader than expected from diffusion-limited aggregation theory, at least in the biological media reported here. These results will be useful for nanotoxicity studies or other experiments in which it is necessary to know how the agglomeration state changes with time or in different media. Sedimentation coefficient distributions measured by AUC could also be useful for predicting depletion rates of agglomerates from solution in environmental systems for nanotoxicity studies and the probability of large concentration increases at, for example, the cell layer in a well-plate study. Although the focus of this work was agglomeration of AuNPs, we expect AUC to be useful for measuring agglomeration of the numerous other types of NPs previously measured as single NPs by AUC including Ag, CdSe, TiO_2, Fe_3O_4, $ZrSO_4$, and any others that can be measured by either absorbance or interference.[13−16]

We also successfully used AUC to measure the absorbance spectra of size-differentiated AuNPs. We anticipate that this technique will be useful for providing quantitative data supporting the theory behind changes in the LSPR spectrum during agglomeration and thereby enabling the design of better LSPR-based biosensors using ligand-coated AuNPs and AgNPs. We also demonstrated that the spectra measured by AUC can subsequently be used to rapidly estimate the size distribution of small AuNP agglomerates simply from the bulk absorbance spectrum of other solutions not measured by AUC.

MATERIALS/METHODS

Materials (ref 27). Nominal 10 and 30 nm AuNPs (Part #15703, #15706, Ted Pella, Redding, CA) were used as received. Dulbecco's modified Eagle's medium (DMEM) with 4.5 g/L glucose and sodium pyruvate but without phenol red or L-glutamine was obtained from Mediatech (Manassas, VA). Bovine serum albumin was from Sigma Aldrich (St. Louis, MO) (≥96%, essentially fatty acid free). The antibiotics streptomycin and penicillin were from Invitrogen and were added at 100 µg/mL and 100 U/mL, respectively, to DMEM to reduce bacterial growth. DMEM + 8% BSA by weight was filtered through a 0.2 µm polypropylene filter to remove large protein aggregates that would interfere with the DLS measurements.

Controlled Agglomeration Procedure. To produce different size distributions of stable NP agglomerates in cell culture media, we use a recently described method.[10] Briefly, the NPs are allowed to agglomerate in DMEM without protein for a specified period of time, and then 1% (final concentration) BSA is added to coat the agglomerates and stop agglomeration. Specifically, to create the agglomerates, we (1) add 225 µL of DMEM to a 1.5 mL centrifuge tube, (2) add 300 µL of AuNPs while vortexing and vortex for 1 to 2 s, (3) wait for the specified period of time, and (4) add 75 µL of DMEM + 8% BSA while vortexing. Note that the precision of the waiting times in step 3 is not critical since the purpose of this procedure is simply to produce different sizes of agglomerates that can then be measured by DLS and AUC. To produce the well-dispersed NPs ("0 s"), we (1)

add 225 µL of DMEM to a 1.5 mL centrifuge tube, (2) add 75 µL of DMEM + 8% BSA, and (3) add 300 µL of AuNPs while vortexing at maximum speed.

DLS and Absorbance Measurements. After dispersing the NPs in cell culture media, the NPs were measured by DLS and UV−visible−near IR absorbance prior to the AUC measurements. DLS was performed using a Brookhaven Instruments (Holtsville, NY, USA) ZetaPALS with a 660 nm laser and the detector at 90°. The combined mean size after 100 s was compensated for vibration and rotation and used in the DLCA calculations described above. Bulk absorbance measurements were made using a Hewlett-Packard 8453 spectrophotometer, measuring from 190 to 1100 nm and integrating for 0.5 s.

AUC Measurements. AUC measurements were made with a Beckman-Coulter XL-I (Brea, CA). The cell was equilibrated at 20 °C. The reference cell was filled with a solution equivalent to the measuring cell except without NPs.

For the size distribution measurements, radial scans were performed as frequently as possible measuring at the peak wavelength 526 nm, with a radial step size of 0.005 cm. For the 30 nm AuNPs, the rotor speed was set to provide a relative centrifugal force (rcf, relative to gravity) of 88 (1100 rpm) for the 30 s and 2 min agglomerates, 105 (1200 rpm) for the 10 s agglomerates, 291 (2000 rpm) for the 2 s agglomerates, 352 (2200 rpm) for the NPs in water, and 455 (2500 rpm) for the 0 s well-dispersed NPs. For the 10 nm AuNPs, the rcf was set to 88 (1100 rpm) for the 10 s agglomerates, 16 400 (15 000 rpm) for the NPs in water, and 29 100 (20 000 rpm) for the 0 s

well-dispersed NPs. The radial scans were analyzed with the $c(s)$ and ls-$g^*(s)$ algorithms in Sedfit, fitting the baseline with a resolution of 100 and confidence level of 0.95. The s distributions were then exported to be converted to M and r_h distributions and compared with DLCA theory in Matlab.

For the AUC absorbance spectrum measurements, wavelength scans were performed as frequently as possible at a radial position of 6.8 cm and measuring every 1 nm from 450 to 800 nm (although the AUC frequently took larger steps than 1 nm so that the mean step size was about 1.8 nm). The radial position of 6.8 cm was chosen because the ratio of separation by sedimentation coefficient to spreading by diffusion increases with radial position, and it is sufficiently far from the outside of the cell to neglect any edge effects. The reference cell contained a 1:1 solution of water and DMEM + 1% BSA. The rotor speed was set to provide an rcf of 88 (1100 rpm) for the 30 s and 2 min agglomerates, 105 (1200 rpm) for the 9 and 10 s agglomerates, 325 or 455 (2200 or 2500 rpm) for the 3 and 2 s agglomerates, and 455 (2500 rpm) for the 0 s well-dispersed NPs. Wavelength scans were collected until the baseline was reached (generally between 90 and 120 min). After the last wavelength scan was completed, a single radial scan was run in order to estimate the position of the meniscus for each sample (which depends on the precise volume injected).

Estimating Agglomerate Size Distribution from Bulk Absorbance Spectrum. After calculating the absorbance spectrum for each agglomerate size, we hypothesized that we may be able to estimate the agglomerate size distribution simply from a fast measurement of the bulk absorbance spectrum. The bulk absorbance spectrum should be a linear combination of the spectra for the individual agglomerate sizes, so the concentration of each agglomerate size could be estimated if the spectra are sufficiently independent. Because the spectra for different sizes of agglomerates are not completely independent, especially for larger agglomerates, we used the constrained least-squares linear equation solver in Matlab, with the constraint that the size distribution should be either smoothly decreasing for all M or smoothly increasing and then decreasing, and all concentrations must be non-negative. Specifically, for both the 1 and 2 s agglomerates, the constraints used to obtain a smoothly decreasing size distribution were that $C_{n+1} < 0.8C_n$ for $3 < n < 9$, where C_n is the concentration of the agglomerate of size $M = (1, 2, 3, 4, 5, 7, 10, 15, 20)$, with n corresponding to the position in the series in parentheses.

TEM Measurements. For the transmission electron microscopy measurements, TEM samples were prepared by pipetting two 15 μL samples of the undiluted AuNP sample in DMEM$-$BSA onto a holey carbon-coated copper grid (SPI supplies, West Chester, PA, USA) and allowed to evaporate overnight. Transmission electron microscopy measurements were performed with a JEOL 9 100 CX electron microscope equipped with an IA L9C camera. For each sample, a minimum of 10 pictures were taken at 100 000$\times$ magnification and 80 kV. The TEM was calibrated using both waffle grating (462.9 nm) and catalase crystal (8.75 nm) TEM calibration standards. Both standards were purchased from Electron Microscopy Sciences (Hatfield, PA, USA).

AFM Measurements. For the atomic force microscopy measurements, 20 μL of the undiluted AuNP samples in DMEM$-$BSA was pipetted onto a 5 mm by 5 mm amine-functionalized Si wafer AFM substrate (see NIST-NCL PCC-6 for further chemistry details on substrate preparation). The AuNPs were allowed to incubate for 1 h, washed with deionized water, and dried with pressurized nitrogen in order to minimize additional agglomeration resulting from drying the sample on the surface. A Dimension 3100 instrument with a Nanoscope V controller (Bruxer AXS, Santa Barbara, CA, USA) was operated in intermittent-contact mode using an open-loop scanner. AFM tips with a vendor-reported radius of curvature of 10 nm and a nominal spring constant of 5 N m^{-1} were used (Tap150-Al-G, NanoAndMore, Lady Island, SC). Ten images were collected per substrate. Sizing results were obtained using a MatLab routine and procedure previously described by Boyd and Cuenat.[28] Sizes are reported as the mean of all particles measured, with one standard deviation about the mean.

Theory. *Diffusion-Limited Colloidal Aggregation.* DLCA theory models aggregation/agglomeration processes by assuming that NPs stick permanently as soon as they encounter each other by diffusion. It has been used successfully to explain the increase in size of AuNP agglomerates measured using DLS, although the DLS measurement had to be compensated for vibration and rotation of the agglomerates.[10,20] DLCA theory can also predict the distribution of the number of particles per agglomerate,[20] which can be converted to a mass-weighted size distribution as described recently.[10]

Analytical Ultracentrifugation. Since particles of a particular size and density form a vertical sedimentation boundary (in the absence of diffusion or other dispersion) that moves from smaller to larger radii during centrifugation, AUC can be used to estimate the sedimentation coefficient distribution of a sample by measuring the absorbance at various radial positions within a cell over time while the cell is being centrifuged. The sedimentation coefficient is a function of the density and size of the NP agglomerate as described by equation S2 in the Supporting Information. The density of bare AuNPs was assumed to be the same as bulk gold (19.3 g/mL), and 1.37 g/mL was used as the density of BSA, from which the Supporting Information describes how the density of protein-coated AuNPs was calculated. The Supporting Information also includes a derivation of the equations we used to calculate how sedimentation coefficients depend on the size of protein-coated NPs and protein-coated fractal-shaped NP agglomerates. Then, we calculated the NP and agglomerate size distributions from AUC radial scan measurements (*e.g.*, Figure 4a). After calculating the agglomerate size from the sedimentation coefficient and determining that diffusion is negligible for agglomerates, we measured the changes in absorbance spectrum over time using the AUC in wavelength scan mode at a single radial position (see Figure 4b). Since diffusion is negligible, the sedimentation boundary for a single agglomerate size passes through the measured radial position at each time. Therefore, we could use the AUC wavelength scan measurements to calculate the absorbance spectrum of each agglomerate size from the smoothed time derivative of the absorbance spectrum corrected for the wedged shape of the AUC cell, as described in the Supporting Information. The Supporting Information includes the Matlab scripts used to perform all the above calculations.

Absorbance-Weighted vs Mass-Weighted Size Distributions. Size distributions obtained from AUC absorbance measurements are weighted by the absorbance of the agglomerates at the measured wavelength. In this work, we measure the absorbance at 526 nm, which is the peak absorbance of unagglomerated gold NPs. The absorbance at 526 nm decreases with agglomeration, although it changes only slightly after agglomerates reach a certain size, as seen in Figure 1. Therefore, the absorbance-weighted size distributions we obtain from AUC are weighted more toward smaller agglomerates than the mass-weighted size distributions obtained from DLCA theory.

Supporting Information Available: Additional theory and figures to explain how the AUC data were analyzed, as well as the Matlab scripts used to carry out the calculations. This material is available free of charge via the Internet at http://pubs.acs.org.

REFERENCES AND NOTES

1. Elghanian, R.; Storhoff, J. J.; Mucic, R. C.; Letsinger, R. L.; Mirkin, C. A. Selective Colorimetric Detection of Polynucleotides Based on the Distance-Dependent Optical Properties of Gold Nanoparticles. *Science* **1997**, *277*, 1078–1081.

2. Peng, H. I.; Miller, B. L. Recent Advancements in Optical DNA Biosensors: Exploiting the Plasmonic Effects of Metal Nanoparticles. *Analyst* **2011**, *136*, 436–447.

3. Rastogi, V.; Velev, O. D. Development and Evaluation of Realistic Microbioassays in Freely Suspended Droplets on a Chip. *Biomicrofluidics* **2007**, *1*, 17.

4. Cao, Y. W. C.; Jin, R. C.; Mirkin, C. A. Nanoparticles with Raman Spectroscopic Fingerprints for DNA and RNA Detection. *Science* **2002**, *297*, 1536–1540.

5. Roca, M.; Haes, A. J. Probing Cells With Noble Metal Nanoparticle Aggregates. *Nanomedicine* **2008**, *3*, 555–565.

6. Schulze, C.; Kroll, A.; Lehr, C. M.; Schafer, U. F.; Becker, K.; Schnekenburger, J.; Isfort, C. S.; Landsiedel, R.; Wohlleben, W. Not Ready To Use - Overcoming Pitfalls When Dispersing Nanoparticles in Physiological Media. *Nanotoxicology* **2008**, *2*, 51–U17.

7. Jiang, J. K.; Oberdorster, G.; Biswas, P. Characterization of Size, Surface Charge, and Agglomeration State of Nanoparticle Dispersions for Toxicological Studies. *J. Nanopart. Res.* **2009**, *11*, 77–89.

8. Elzey, S.; Grassian, V. H. Agglomeration, Isolation and Dissolution of Commercially Manufactured Silver Nanoparticles in Aqueous Environments. *J. Nanopart. Res.* **2010**, *12*, 1945–1958.

9. MacCuspie, R. I. Colloidal Stability of Silver Nanoparticles in Biologically Relevant Conditions. *J. Nanopart. Res.* **2011**, *13*, 2893–2908.

10. Zook, J. M.; Maccuspie, R. I.; Locascio, L. E.; Halter, M. D.; Elliott, J. T. Stable Nanoparticle Aggregates/Agglomerates of Different Sizes and the Effect of Their Size on Hemolytic Cytotoxicity. *Nanotoxicology* **2011**, in press, DOI: 10.3109/17435390.2010.536615.

11. Laue, T. M.; Stafford, W. F. Modern Applications of Analytical Ultracentrifugation. *Annu. Rev. Biophys. Biomol. Struct.* **1999**, *28*, 75–100.

12. Lebowitz, J.; Lewis, M. S.; Schuck, P. Modern Analytical Ultracentrifugation In Protein Science: A Tutorial Review. *Protein Sci.* **2002**, *11*, 2067–2079.

13. Calabretta, M.; Jamison, J. A.; Falkner, J. C.; Liu, Y. P.; Yuhas, B. D.; Matthews, K. S.; Colvin, V. L. Analytical Ultracentrifugation for Characterizing Nanocrystals and Their Bioconjugates. *Nano Lett.* **2005**, *5*, 963–967.

14. Colvin, V. L.; Jamison, J. A.; Yavuz, C. T.; Redden, J. J.; Krueger, K. M.; Mayo, J. T. Applying Analytical Ultracentrifugation to Nanocrystal Suspensions. *Nanotechnology* **2009**, 355702.

15. Falabella, J. B.; Cho, T. J.; Ripple, D. C.; Hackley, V. A.; Tarlov, M. J. Characterization of Gold Nanoparticles Modified with Single-Stranded DNA Using Analytical Ultracentrifugation and Dynamic Light Scattering. *Langmuir* **2010**, *26*, 12740–12747.

16. Planken, K. L.; Colfen, H. Analytical Ultracentrifugation of Colloids. *Nanoscale* **2010**, *2*, 1849–1869.

17. Grobelny, J.; Delrio, F. W.; Pradeep, N.; Kim, D.-I.; Hackley, V. A.; Cook, R. F. *NIST - NCL Joint Assay Protocol PCC-6*. http://ncl.cancer.gov/working_assay-cascade.asp.

18. Keene, A.; Tyner, K. Analytical Characterization of Gold Nanoparticle Primary Particles, Aggregates, Agglomerates, and Agglomerated Aggregates. *J. Nanopart. Res.* **2011**, *13*, 3465–3481.

19. Geronimo, C. L. A.; MacCuspie, R. I. Antibody-Mediated Self-Limiting Self-Assembly for Quantitative Analysis of Nanoparticle Surfaces by Atomic Force Microscopy. *Microsc. Microanal.* **2011**, *17*, 206–214.

20. Lin, M. Y.; Lindsay, H. M.; Weitz, D. A.; Klein, R.; Ball, R. C.; Meakin, P. Universal Diffusion-Limited Colloid Aggregation. *J. Phys.: Condens. Matter* **1990**, *2*, 3093–3113.

21. Tsai, D.-H.; Cho, T. J.; DelRio, F. W.; Taurozzi, J.; Zachariah, M. R.; Hackley, V. A. Hydrodynamic Fractionation of Finite Size Gold Nanoparticle Clusters. *J. Am. Chem. Soc.* **2011**, *133*, 8884–8887.

22. Naeimi, Z.; Miri, M. Optical Properties of Fractal Aggregates of Nanoparticles: Effects of Particle Size Polydispersity. *Phys. Rev. B* **2009**, *80*.

23. Jain, P. K.; Huang, W. Y.; El-Sayed, M. A. On The Universal Scaling Behavior of the Distance Decay of Plasmon Coupling in Metal Nanoparticle Pairs: A Plasmon Ruler Equation. *Nano Lett.* **2007**, *7*, 2080–2088.

24. Messina, E.; Cavallaro, E.; Cacciola, A.; Iati, M. A.; Gucciardi, P. G.; Borghese, F.; Denti, P.; Saija, R.; Compagnini, G.; Meneghetti, M.; Amendola, V.; Marago, O. M. Plasmon-Enhanced Optical Trapping of Gold Nanoaggregates with Selected Optical Properties. *ACS Nano* **2011**, *5*, 905–913.

25. Schuck, P. Size-Distribution Analysis of Macromolecules by Sedimentation Velocity Ultracentrifugation and Lamm Equation Modeling. *Biophys. J.* **2000**, *78*, 1606–1619.

26. Quinten, M.; Kreibig, U. Optical-Properties of Aggregates of Small Metal Particles. *Surf. Sci.* **1986**, *172*, 557–577.

27. Certain commercial equipment, instruments, or materials are identified in this report to specify adequately the experimental procedure. Such identification does not imply recommendation or endorsement by the National Institute of Standards and Technology, nor does it imply that the materials or equipment identified are necessarily the best available for the purpose.

28. Boyd, R. D.; Cuenat, A. New Analysis Procedure for Fast and Reliable Size Measurement of Nanoparticles from Atomic Force Microscopy Images. *J. Nanopart. Res.* **2011**, *13*, 105–113.